

Experimental Test of Universality of the Anderson Transition

Matthias Lopez,¹ Jean-François Clément,¹ Pascal Szriftgiser,¹ Jean Claude Garreau,¹ and Dominique Delande²

¹*Laboratoire de Physique des Lasers, Atomes et Molécules,*

*Université Lille 1 Sciences et Technologies, CNRS; F-59655 Villeneuve d'Ascq Cedex, France**

²*Laboratoire Kastler-Brossel, UPMC-Paris 6, ENS, CNRS; 4 Place Jussieu, F-75005 Paris, France*

(Dated: August 22, 2011)

We experimentally test the universality of the Anderson three dimensional metal-insulator transition. Nine sets of parameters controlling the microscopic details of this second order phase transition have been tested. The corresponding critical exponents are independent (within 2σ) of these microscopic details, and the average value 1.63 ± 0.05 is in very good agreement with the numerically predicted value, $\nu = 1.58$.

PACS numbers: 72.15.Rn, 03.75.-b, 05.45.Mt, 64.70.Tg

In the presence of a disordered potential, the classical diffusive transport of a particle can be inhibited by quantum interference among the various paths where the particle is multiply scattered by disorder, a puzzling phenomenon known as Anderson localization [1]. The dimensionality of the system plays a major role, which can be understood qualitatively from the scaling theory of localization [2]. In dimension $d = 3$ and above, there is a delocalized-localized (or metal-insulator in solid-state physics language) transition — known as the Anderson transition. An energy “mobility edge” E_c , which is a decreasing function of disorder, separates localized motion at low energy from diffusive motion at high energy. On the localized side, the localization length ξ diverges algebraically $\xi(E) \propto (E_c - E)^{-\nu}$, with ν the critical exponent of the transition. On the diffusive side, the diffusion constant vanishes like $D(E) \propto (E - E_c)^s$ with, according to the scaling theory, $s = (d-2)\nu$ [2, 3]. A key prediction of the scaling theory is that the critical exponents are **universal**, that is, they do not depend on the microscopic details of the system, such as the correlation functions of the disorder, the dispersion relation of the particles, etc. Numerical experiments on simple models [4–6] such as the tight-binding Anderson model, have confirmed this universality, with a non-trivial value of the critical exponent around $\nu = 1.58$ for spinless time-reversal invariant 3-dimensional (3D) systems [7]. However, there is a huge lack of experimental results. In this letter, we present accurate measurements of the critical exponent ν in 3D, and, by varying the various experimental parameters, test whether its value is universal.

Anderson localization is due to interference between long multiple scattering paths and is thus very sensitive to any mechanism destroying the phase coherence of the wavefunction, making its experimental observation and characterization very difficult [8]. In the context of electronic transport in disordered samples, electron-electron interaction is sufficiently important to partly invalidate the one-body Anderson scenario, leading to a critical exponent close to unity [9]. In a slightly different context, Anderson localization of acoustic [10] and electromag-

netic [11–13] waves has been experimentally observed. There, absorption is a limitation, and the critical exponent $\nu \approx 0.5$ estimated in [13] does not agree with the numerical simulation result 1.58.

Cold atomic gases are conceptually simple systems which can be exposed to well controlled disorder. For sufficiently cold samples, the phase coherence time of the wavefunction describing the center of mass motion can be kept sufficiently long for atomic interferometry experiments to be routinely performed. Atom-atom interaction can be reduced to a minimum, either by using dilute cold gases, or by using a Feshbach resonance [14]. Direct observation of Anderson localization of atomic matter waves *in a one-dimensional* disordered [15] or quasi-periodic [16] potential has been reported, the disordered potential being created by the effective interaction with a detuned laser beam with a random spatial profile (speckle). Very recently, observations of the Anderson localization in a 3D atomic gases have been claimed [17]. However, the interpretation of both results involves heuristic assumptions, and a better understanding is needed before the observation of a mobility edge can be asserted.

This difficulty prompted the use of a slightly different system, where the disordered potential is replaced by classical chaotic dynamics. In the kicked rotor, a paradigmatic system of quantum chaos, quantum mechanical interference tend to suppress the classical chaotic diffusive dynamics, and to induce a phenomenon originally called *dynamical localization*, later discovered to be an analog of 1D Anderson localization *in momentum space*, by mapping the kicked rotor onto a quasirandom 1D Anderson model [18]. The experimental realization of the kicked rotor with laser-cooled atoms interacting with a pulsed standing wave allowed the first experimental observation of Anderson localization in 1D with atomic matter waves [19]. In order to observe the Anderson *transition*, however, an analog of the 3D Anderson model is needed [20]. Here, we focus on the so-called “quasi-periodic kicked rotor” in which three incommensurate frequencies are used to generate the 3D character [21], and shown in [22] to be

strictly equivalent to an anisotropic 3D Anderson model, a fact further confirmed by a low-energy effective field theory [23]. Meticulous numerical experiments [6] have shown the universality of the critical exponent for this system, $\nu = 1.58 \pm 0.02$, in excellent agreement with values found in the literature for the Anderson model [4].

An experiment based on this system has characterized the Anderson metal-insulator transition [24], with the first experimental determination of the critical exponent $\nu = 1.4 \pm 0.3$. The experimental setup, described in detail in [22] consists of laser-cooled cesium atoms interacting with a pulsed far-detuned standing wave (wavenumber $k_L = 7.4 \times 10^6 \text{ m}^{-1}$ and maximum one-way intensity 180 mW). The amplitude of the kicks is modulated with two frequencies ω_2 and ω_3 . The Hamiltonian reads:

$$H = \frac{p^2}{2} + K \cos x [1 + \varepsilon \cos(\omega_2 t) \cos(\omega_3 t)] \sum_{n=0}^{N-1} \delta(t - n), \quad (1)$$

where time is measured in units of the kicking period T_1 , space in units of $(2k_L)^{-1}$, momentum in units of $2\hbar k_L/\bar{k}$, with $\bar{k} = 4\hbar k_L^2 T_1/M$ (M is the atom mass) playing the role of an effective Planck constant ($[x, p] = i\bar{k}$) and K is the average kick amplitude. The kicks are short enough (duration $\tau = 0.8 \mu\text{s}$) compared to the atom dynamics to be considered as Dirac delta functions. If ω_2, ω_3, π and \bar{k} are incommensurate, this 1D quasiperiodic kicked rotor has a 3D Anderson metal-insulator transition, displaying localization in *momentum space*. Compared to [24] and [22], the signal to noise and the stability of the experiment have been greatly improved. Atomic momentum is measured by Raman stimulated transitions. The previous Raman frequency generation setup used direct current modulation of a master laser diode to drive the Raman slave lasers [25]. This system has been replaced by a fibered phase modulator driven at 9.2 GHz. Moreover, 3 (of 4) master diode lasers working with an external cavity setup have been replaced by distributed feedback lasers, extending the experiment stability from a few hours to several days. These improvements lead to much better experimental signals, making the determination of the critical exponent much more accurate and reliable, opening the possibility to test its universality.

A Sisyphus-boosted magneto-optical trap prepares an initial thermal state of FWHM $4 \times 2\hbar k_L$, much narrower than the final (localized or diffusive) momentum distribution, and – by time-reversal symmetry – $\langle p(t) \rangle$ remains zero at all time t . We can directly monitor the dynamics rather than rely on “bulk” quantities such as the conductance, itself related to the diffusion constant. A good quantity characterizing the dynamics is $\langle p^2(t) \rangle$. For practical and historical reasons, the atomic momentum P is measured in units of two recoil momenta:

$$\mathbf{p} = \frac{P}{\bar{k}} = \frac{P}{2\hbar k_L}. \quad (2)$$

	\bar{k}	$\frac{\omega_2}{2\pi}$	$\frac{\omega_3}{2\pi}$	Path in (K, ε)	K_c	ν
A	2.89	$\sqrt{5}$	$\sqrt{13}$	4,0.1 \rightarrow 8,0.8	6.67	1.63 ± 0.06
B	2.89	$\sqrt{7}$	$\sqrt{17}$	4,0.1 \rightarrow 8,0.8	6.68	1.57 ± 0.08
C	2.89	$\sqrt{5}$	$\sqrt{13}$	3,0.435 \rightarrow 10,0.435	5.91	1.55 ± 0.25
D	2.89	$\sqrt{5}$	$\sqrt{13}$	7.5,0 \rightarrow 7.5,0.73	$\varepsilon_c=0.448$	1.67 ± 0.18
E	2.00	$\sqrt{5}$	$\sqrt{13}$	3,0.1 \rightarrow 5.7,0.73	4.69	1.64 ± 0.08
F	2.31	$\sqrt{5}$	$\sqrt{13}$	4,0.1 \rightarrow 9,0.8	6.07	1.68 ± 0.06
G	2.47	$\sqrt{5}$	$\sqrt{13}$	4,0.1 \rightarrow 9,0.8	5.61	1.55 ± 0.10
H	3.46	$\sqrt{5}$	$\sqrt{13}$	4,0.1 \rightarrow 9,0.8	6.86	1.66 ± 0.12
I	3.46	$\sqrt{5}$	$\sqrt{13}$	4,0.1 \rightarrow 9,0.8	7.06	1.70 ± 0.12

Table I: The 9 sets of parameters used: \bar{k} , ω_2 and ω_3 control the microscopic details of the disorder, K controls the amplitude and ε the anisotropy of the hopping amplitudes. The critical point K_c depends on the various parameters but the critical exponent is universal. The weighted mean of the critical exponent is $\nu = 1.63 \pm 0.05$. The duration of the kicks is $\tau = 0.8 \mu\text{s}$ for sets A-H, and $\tau = 0.96 \mu\text{s}$ for set I.

In the diffusive regime, $\langle \mathbf{p}^2(t) \rangle$ increases linearly with time; in the localized regime, it saturates at long times to a value proportional to the square of the localization length. In [22], it was shown that, in order to characterize the Anderson transition, one should measure:

$$\Lambda(t) = \langle \mathbf{p}^2(t) \rangle t^{-2/3}. \quad (3)$$

$\Lambda(t)$ scales like $t^{-2/3}$ in the localized regime, like $t^{1/3}$ in the diffusive regime and is *constant* in the critical intermediate regime. By measuring $\Lambda(t)$, one has thus a direct access to the state of the system. K is a control parameter playing the role of the energy in the Anderson model. The critical value K_c is a mobility edge separating a localized regime at low K from a diffusive regime at large K . The critical exponent ν can be determined from the algebraic divergence $1/(K_c - K)^\nu$ of the localization length near the critical point. For fixed $\bar{k}, \omega_2, \omega_3$, one can also chose a path in the (K, ε) plane which crosses the critical line “at right angle”, i.e. faster, which improves the accuracy on the critical exponent. Rather than measuring the full momentum distribution to obtain $\langle \mathbf{p}^2(t) \rangle$, we measure the atomic population in the zero-momentum class $\Pi_0(t)$. As shown in [26], $\langle \mathbf{p}^2(t) \rangle$ is, by conservation of the number of atoms, proportional to $\Pi_0^{-2}(t)$. The precise proportionality factor depends on the shape of the momentum distribution, which has been shown experimentally [26] to vary smoothly across the transition. The quantity measured experimentally, $\Lambda_{\text{exp}}(K, t) = \Pi_0^{-2}(K, t)t^{-2/3}$, has the same critical point and the same critical exponent than Eq. (3). In the simplest experiment, parameters $\bar{k}, \omega_2, \omega_3, \varepsilon$ are fixed and $\Pi_0(K, t)$ recorded for several values of the control parameter K , from which $\Lambda_{\text{exp}}(K, t)$ is obtained.

As one cannot pursue the experiment for arbitrary long times, making the distinction between the true critical point where $\Lambda_{\text{exp}}(K_c, t)$ is a constant and a neighboring

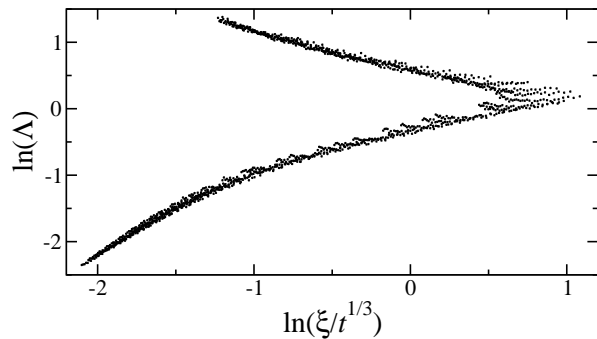


Figure 1: Typical scaling function constructed from the experimental data measured on the quasi-periodic kicked rotor (set E of Tab. I). The tip on the right side indicates the critical point of the Anderson transition, the diffusive (resp. localized) regime is the upper (resp. lower) branch. The dispersion of the points is an indication of the uncertainty on the measured data.

point of small positive (localized) or small negative (diffusive) slope is difficult. To circumvent this, we use the finite-time scaling procedure explained in [22], which is a simple extension to the time domain of the finite-size scaling method used in solid-state physics [27]. We assume that there exists a scaling function F such that:

$$\Lambda_{\text{exp}}(K, t) = F\left(\xi(K)t^{-1/3}\right) \quad (4)$$

where $\xi(K)$ is an unknown function to be determined. The idea, described in detail in [22, 28] is that $\xi(K)$ should be chosen so that $F(\xi(K)t^{-1/3})$ is a continuous function, safe for the divergence at the critical point, with two distinct localized and diffusive branches. In order to do so, we try to collapse the various experimental curves $\Lambda_{\text{exp}}(K, t)$, corresponding to each value of K , in a single curve, the various $\xi(K)$ - associated to the localization length on the localized branch - being free fitting parameters. A typical scaling function is shown in Fig. 1 and the corresponding fit parameter function ξ in Fig. 2. Comparison with our previously published data, e.g. Fig. 3(c) in [24], shows a dramatic improvement in the quality of the measurements. Each point $\Lambda_{\text{exp}}(K, t)$ results from independent experiments, making the statistical errors rather easy to evaluate. We checked that the dispersion of points around the scaling function in Fig. 1 is of the order of $\Delta(\ln \Lambda) \approx 0.05$, limited by the experimental uncertainties, the χ^2 per degree of freedom of the fit being typically slightly smaller than 1.

From finite-time measurements, it is impossible to extract a truly diverging $\xi(K)$. Several spurious phenomena [22] are responsible for the observed cut-off: The dominant one is the finite duration of the experiment. Several sources of decoherence, such as spontaneous emission, collisions between atoms, residual effect of gravity because the laser beams are not perfectly horizontal, and the inhomogeneity related to the Gaussian inten-

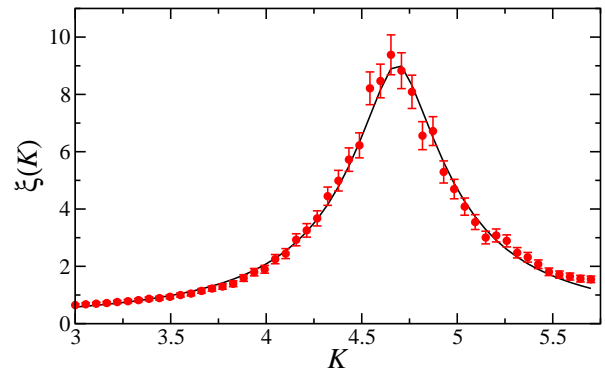


Figure 2: (color on line) Red points with error bars: Characteristic length $\xi(K)$ constructed from the experimental data (set E of Tab. I). At low K (localized regime), it is proportional to the localization length. At large K (diffusive regime), it is inversely proportional to the diffusion constant. The “divergence” near $K_c = 4.69$ is a signature of a second order quantum phase transition. Several phenomena limit this divergence, see text for discussion. They are taken into account by a fit including a cut-off parameter, Eq. (5), shown as a solid curve, from which the critical exponent ν is extracted.

sity profile of the standing wave contribute to the cut-off. We have increased the phase coherence time up to 200-300 kick periods, in agreement with theoretical calculations [22]. In order to reduce uncontrolled systematic effects, we chose to use the same time interval - from 30 to 150 kicks - for the analysis of all experimental data. The finite duration is also responsible for systematic effects: It tends to slightly underestimate K_c , but does not seem to shift significantly the critical exponent. Using a different interval, 30-120 kicks, produces ν values not differing by more than 0.05.

A typical $\xi(K)$ curve, Fig. 2, displays a clear “divergence” near the critical point (increase by more than one order of magnitude, much better than in [24]). It is itself fitted to extract the position of the critical point K_c and the critical exponent ν , using the following formula:

$$1/\xi(K) = \alpha|K - K_c|^\nu + \beta \quad (5)$$

where β is a cut-off parameter taking into account the various limitations discussed above. As seen in Fig. 2 the fit is excellent. The fitting parameter ν depends on the range of K where the fit is performed. A too small range produces a large uncertainty in ν while the quality of the fit deteriorates for a too large range. To avoid any bias, we have fitted all data sets in the interval $[0.8K_c, 1.2K_c]$, for which the χ^2 per degree of freedom is of the order of 1. The uncertainties are calculated using a bootstrap method starting from the raw experimental data and their error bars, ending to the determination of ν through the construction of the scaling function. For data sets presented, no statistically significant anomaly has been detected. The statistical uncertainty on K_c is very small, at most few 10^{-2} , but the finite duration of

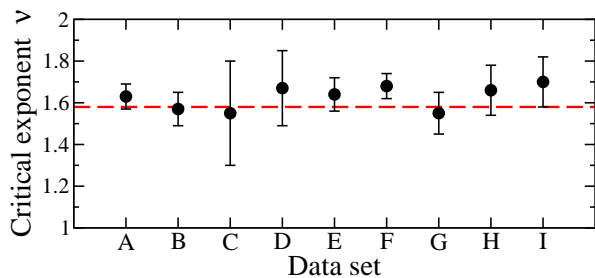


Figure 3: (color online) Experimental test of the universality of the metal-insulator transition. The critical exponent ν , measured for 9 different sets of parameters A-I, is *universal*, i.e. independent of the microscopic details. The error bars indicate one standard deviation, measured using the experimental uncertainties and a bootstrap technique. The horizontal dashed line is the commonly accepted value $\nu = 1.58$, determined from extensive numerical calculations on various models. Parameter values: See Tab. I.

the experiment is responsible for a systematic shift towards low K (see above).

In order to test the universality of the critical exponent, we have chosen a “reference” set of parameters, noted A in table I, which has the same parameters used in [24]. We have then modified the ω_2 and ω_3 frequencies for set B. We have also modified the path in the (K, ε) plane, either by changing K only (set C) or ε only (set D). In these two situations, the crossing of the critical regime is slower, making the accuracy on ν significantly worse. We have further modified the kicking period T_1 , which affects the effective Planck’s constant \hbar . Several smaller \hbar values have been used in sets E, F and G. One larger value of \hbar was used in sets H and I the difference between the two sets being the duration of the laser pulses. The fact that very close values of K_c and the same critical exponent are obtained is a strong indication that our experimental system is well described by the model Hamiltonian, Eq. (1).

The final results are given in table I and plotted with their error bars (one standard deviation) in Fig. 3. They unambiguously demonstrate the universality of the localized-diffusive transition in the quasi-periodic kicked rotor. Moreover, all numerical values are compatible (within 2 standard deviations) with the best numerical determinations of $\nu = 1.58 \pm 0.02$, both for the kicked rotor and the Anderson model. They all markedly differ from the value 1 predicted by the self-consistent theory of localization [29]. The later theory is an attempt to justify the scaling properties using a microscopic approach: It is qualitatively correct and gives simple physical pictures. For example, it has been used to successfully predict the momentum distribution at the critical point [26]. However, it lacks a key ingredient: At criticality, the wavefunctions display very large fluctuations which can be characterized by a multifractal spectrum [7, 30, 31]. Huge fluctuations are known to affect critical exponents of ther-

modynamic phase transitions, it is thus no surprise that they also affect the Anderson transition. While quantum phase transitions are usually considered for the ground state of the system, it must be emphasized that the Anderson transition deals with excited states in the vicinity of the mobility edge, displaying much richer properties. Especially, ultra-cold atomic gases open the way to experimental studies of the interplay of disorder, interference and interactions.

We thank G. Lemarié for useful discussions, and R. Holliger for help with the experiments.

* URL: www.phlam.univ-lille1.fr/atfr/cq

- [1] P. W. Anderson, Phys. Rev. **109**, 1492 (1958).
- [2] E. Abrahams *et al.*, Phys. Rev. Lett. **42**, 673 (1979).
- [3] F. Wegner, Z. Phys. **B25**, 327 (1976).
- [4] K. Slevin and T. Ohtsuki, Phys. Rev. Lett. **82**, 382 (1999).
- [5] F. Milde *et al.*, Eur. Phys. J. B **15**, 685 (2000).
- [6] G. Lemarié, B. Grémaud, and D. Delande, EPL **87**, 37007 (2009).
- [7] F. Evers and A. D. Mirlin, Rev. Mod. Phys. **80**, 1355 (2008).
- [8] M. Janssen, Phys. Rep. **295**, 1 (1998).
- [9] S. Katsumoto *et al.*, J. Phys. Soc. Jap. **56**, 2259 (1987).
- [10] H. Hefei *et al.*, Nature Physics **4**, 945 (2008).
- [11] A. A. Chabanov, M. Stoytchev, and A. Z. Genack, Nature (London) **404**, 850 (2000).
- [12] D. S. Wiersma *et al.*, Nature (London) **390**, 671 (1997).
- [13] M. Störzer *et al.*, Phys. Rev. Lett. **96**, 063904 (2006).
- [14] C. Chin *et al.*, Rev. Mod. Phys. **82**, 1225 (2010).
- [15] J. Billy *et al.*, Nature **453**, 891 (2008).
- [16] G. Roati *et al.*, Nature (London) **453**, 895 (2008).
- [17] S. S. Kondov *et al.*, arXiv:1105.5368v1 [cond-mat.quant-gas] (2011); F. Jendrzejewski *et al.*, arXiv:1108.0137v1 [cond-mat.other] (2011).
- [18] S. Fishman, D. R. Grempel, and R. E. Prange, Phys. Rev. Lett. **49**, 509 (1982); A. Altland and M. R. Zirnbauer, Phys. Rev. Lett. **77**, 4536 (1996).
- [19] F. L. Moore *et al.*, Phys. Rev. Lett. **73**, 2974 (1994).
- [20] J. Wang and A. M. García-García, Phys. Rev. E **79**, 036206 (2009).
- [21] G. Casati *et al.*, Phys. Rev. Lett. **62**, 345 (1989).
- [22] G. Lemarié *et al.*, Phys. Rev. A **80**, 043626 (2009).
- [23] C. Tian, A. Altland, and M. Garst, arXiv:1101.3206v1 [nlin.CD] (2011).
- [24] J. Chabé *et al.*, Phys. Rev. Lett. **101**, 255702 (2008).
- [25] J. Ringot *et al.*, Eur. Phys. J. D **7**, 285 (1999).
- [26] G. Lemarié *et al.*, Phys. Rev. Lett. **105**, 090601 (2010).
- [27] A. MacKinnon and B. Kramer, Phys. Rev. Lett. **47**, 1546 (1981); J. L. Pichard and G. Sarma, J. Phys. C: Solid State Phys. **14**, L127 (1981).
- [28] G. Lemarié, Ph.D. thesis, Université Pierre et Marie Curie, Paris (2009).
- [29] D. Vollhardt and P. Wölffe, in *Electronic Phase Transitions*, edited by W. Hanke and Y.V. Kopayev (Elsevier, Amsterdam, 1992), pp. 1–78.
- [30] J. Martin *et al.*, Phys. Rev. E **82**, 046206 (2010).
- [31] S. Faez *et al.*, Phys. Rev. Lett. **103**, 155703 (2009).